BROADBAND DIELECTRIC SPECTROSCOPY FOR STUDYING MORPHOLOGY AND INTERFACIAL EFFECTS IN POLYMER NANOCOMPOSITES

Polycarpos Pissis, Daniel Fragiadakis, Athanassios Kanapitsas

National Technical University of Athens, Department of Physics, Zografou Campus, 157 80 Athens, Greece

ABSTRACT

Dielectric spectroscopy in the frequency domain and thermally stimulated depolarization currents techniques, covering together a broad frequency range (10^{-4} – 10^{9} Hz), were employed to investigate molecular dynamics in relation to structure and morphology in polymeric nanocomposites. Several systems were investigated, including epoxy resin-modified smectite clay nanocomposites of exfoliated structure, epoxy resin-carbon particle nanocomposites with a mean particle diameter of 3nm, styrene-butadiene rubber-silica nanocomposites and polyimide-silica nanocomposites prepared by sol-gel techniques. Information is obtained from three different regions of the relaxation spectrum, corresponding to local secondary relaxations of the polymer matrix, the cooperative segmental relaxation associated with the glass transition of the polymer matrix and electrical conductivity effects related to the microscopic and macroscopic transport of charge carriers in the nanocomposite. Several interesting results were obtained and discussed for each of the systems studied. Two opposite effects seem to be common to the nanocomposites studied and dominate their behavior: immobilization / reduction of mobility of a fraction of the chains at the interfaces, due to chemical or physical bonds with the particles, and loosened molecular packing of the chains, due to tethering and geometrical confinement, resulting in an increase of free volume.

1. INTRODUCTION

The mechanical and the physical properties of polymer nanocomposites are significantly improved, as compared to those of the polymer matrix, for much smaller filler content than would be required for conventional macroscale or microscale composites [1]. They also exhibit distinctive properties related to the small particle size and correspondingly small mean interparticle spacing (typically also in the nanometer range).

There is yet no satisfactory theoretical explanation for the origin of property improvements in polymer nanocomposites, however it is generally agreed upon that the large surface to volume ratio of the nanoscale inclusions plays a significant role. The presence of an interfacial layer between the bulk polymer and the filler surface, with altered structure and chain mobility, has been established by various techniques [2 – 5]. Many of the properties of the material are strongly dependent on the properties of the interfacial layer. This is due to the fact that this interfacial layer can represent a significant volume fraction of the polymer because of the large surface area presented to the polymer by the nanoparticles.

Dielectric spectroscopy (DS) has proved to b a powerful tool for investigation of the structure and molecular dynamics of polymers and composites. DS is often employed in the framework of the investigation of structure-property relationships in polymeric systems, which provide a basis for the optimization of composition and synthesis/processing conditions for designing new materials with predicted properties. The main advantage of DS, as compared to other similar techniques for studying molecular dynamics, is the broad frequency range, which can be relatively easily covered (10^{-4} – 10^{9} Hz in the present work). This broad frequency range allows to measure on the same sample processes with very different characteristic (relaxation) times and, correspondingly, different characteristic length scales. These include fast secondary (local) relaxations of the polymer matrix at high frequencies with characteristic length scales of below 1nm; cooperative relaxations like the glass transition of the polymer matrix at intermediate frequencies, with characteristic length scales of a few nm (cooperativity length of the glass transition); dc conductivity and conductivity effects (like the interfacial Maxwell-Wagner-Sillars relaxation) at lower frequencies, with characteristic length scales in the nm to μm range.

2. EXPERIMENTAL

2.1. Materials

Details of the preparation and characterization of the materials have been given elsewhere. The nanocomposites investigated include:

(i) epoxy resin-modified smectite clay (ER/clay) nanocomposites of exfoliated structure [8]
(ii) epoxy resin-carbon particle (ER/NCP) nanocomposites with a mean particle diameter of about 3nm [9]
(iii) styrene-butadiene rubber-silica (SBR/silica) nanocomposites [4]
(iv) polyimide-silica (PI/silica) nanocomposites prepared by sol-gel techniques [10, 11]

2.2. Techniques

For broadband DS measurements the complex dielectric function, $\varepsilon=\varepsilon'-i\varepsilon''$, was determined as a function of frequency and temperature. A Schlumberger frequency response analyzer (FRA SI 1260) supplemented with a buffer amplifier of variable gain (Chelsea dielectric interface) in combination with Novocontrol dielectric cells and a Novocontrol Quatro cryosystem was used for measurements in the frequency range 10^{-2} – 10^{6} Hz. For measurements in the 10^{6} – 10^{9} Hz frequency range, a Hewlett-Packard impedance/material analyzer 4291A integrated with a Tabai-Espec temperature chamber SU-240-Y was employed. Details of the measurements and of the various formalisms used for the presentation and analysis of the data have been given elsewhere [8 – 11].

In addition to DS measurements, the non-isothermal dielectric technique of thermally stimulated depolarization currents (TSDC) was used. TSDC consists of measuring the thermally activated release of frozen-in polarization and corresponds to measuring dielectric losses as a function of temperature at low equivalent frequencies of 10^{-2} – 10^{-4} Hz [10]. The method provides a quick characterization of the overall dielectric behavior of the material under investigation and offers advantages of high sensitivity and high resolving power. A Novocontrol TSDC cell in combination with a Keithley 617 electrometer and the Novocontrol Quatro cryosystem was used for measurements in the temperature range from about -150^{o}C to about 400^{o}C.

3. RESULTS AND DISCUSSION

3.1 Overall dielectric response

Fig. 1 shows results obtained with SBR/silica nanocomposites [4]. The composition of SBR was 23.5wt% styrene and 76.5 butadiene. The filler used (30 and 50wt%, nominal) was a precipitated amorphous silica, non-treated (code SV) and pretreated (code SC) to render the surface organophilic [4]. The results show that ε' increases with increasing amount of filler. This can be understood in terms of a higher dielectric constant of the filler than the matrix and effective medium formulae [12] and/or increased molecular mobility of the polymeric chains. An effective medium approach will be discussed later in this section with respect to results obtained with PI/silica hybrid nanocomposites at several filling factors. The values of ε' in the nanocomposites of Fig. 1 exceed, however, those of pure silica (ε' =3.8 – 4.0 at 25^{o}C [11]) indicating that the data can not be explained solely on the basis of mixture formulae. The hypothesis of increased molecular mobility of the polymeric chains resulting from increase of free volume due to loosened molecular packing of the chains confined between the nanoparticles [10] will be further discussed later on the basis of results for the dielectric strength (magnitude) of secondary and primary relaxations.

A dielectric relaxation is observed in Fig. 1 (step in ε'(f)) centered at 10^{6} – 10^{7} Hz. This is the primary α relaxation associated with the glass transition of SBR to be studied in more detail in the next section. The increase in ε'(f) with increasing frequency for $f \leq 10^{3}$ Hz, not observed in the pure matrix, is accompanied by a similar behavior in ε''(f) (not shown). The high values of ε' and ε'' and the low frequencies indicate that these effects originate from

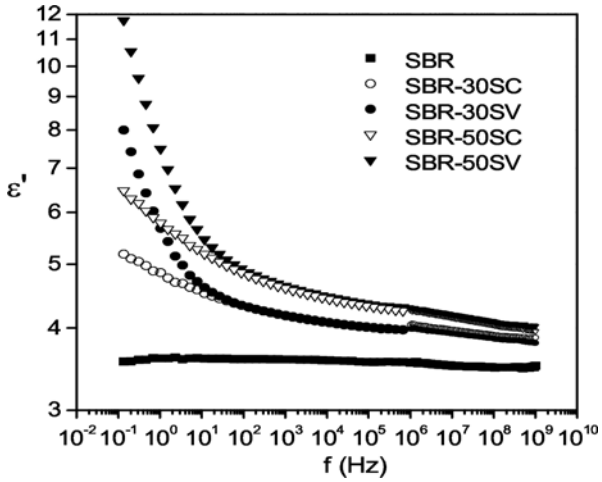

Fig. 1. Real part of dielectric function ε' against frequency f at 25°C for the SBR/silica nanocomposites indicated on the plot

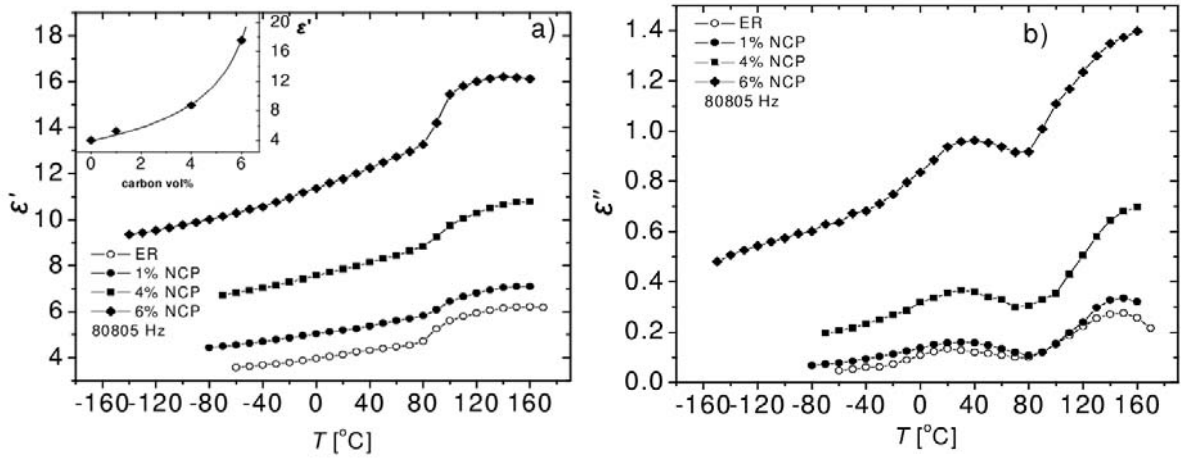

Fig. 2. Temperature dependence of the real ε' (a) and the imaginary part ε'' (b) of the dielectric function of the samples indicated on the plot at 80805 Hz. The inset shows ε' (measured at 1Hz and 50°C) against volume concentration of NCP. The line is a fit of Eq.(1) to the data.

space charge polarization and dc conductivity effects, respectively, in relation to the morphology of the nanocomposites. The results in Fig. 1 show that these effects are more pronounced in the samples with non-treated silica particles, whereas dipolar effects at higher frequencies do not depend on filler treatment. It is reasonable to assume that space charge polarization originates from the accumulation of charges in the volume of polymer trapped within agglomerates formed by the nanoparticles. The higher values of space charge polarization in the composites with non-treated filler suggest then that the degree of agglomeration is larger in these composites. Similar results were obtained with a second formulation of SBR/silica nanocomposites with different chemical treatment, suggesting that low-frequency DS measurements are sensitive to changes in the morphology of the final product induced by chemical treatment of the filler.

Fig. 2 shows results for the temperature dependence of ε' and ε'' in the ER/NCP composites at a constant frequency of 80805 Hz. The data have been recorded isothermally by scanning the frequency and have been replotted here. A relatively high frequency has been chosen for the presentation, in order to eliminate conductivity effects present at lower frequencies. An overall increase of molecular mobility is observed in Fig. 2, in agreement with TSDC data not shown, in the sense that, at each temperature, ε' and ε'' increase with increasing filler content. This is to a large extent related to the formation of a percolation structure of the nanoparticles, as confirmed by the dependence of ε' (at a frequency of 1Hz

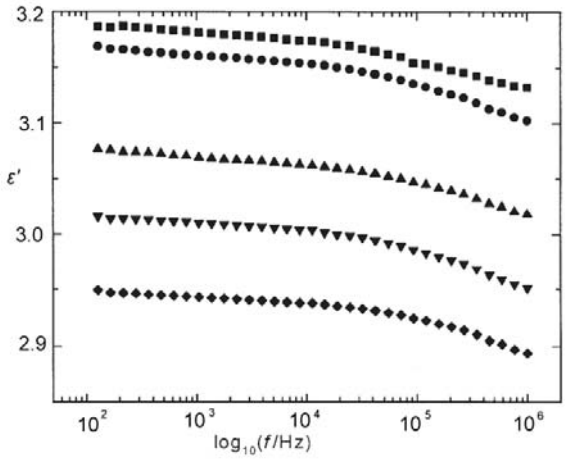

Fig. 3. Frequency dependence of the real part of the dielectric function ε' at 25°C for PI/silica nanocomposites. The weight fraction of silica is from the uppermost to the lowermost curve 0, 8.6, 22.4, 31.7, 35.6

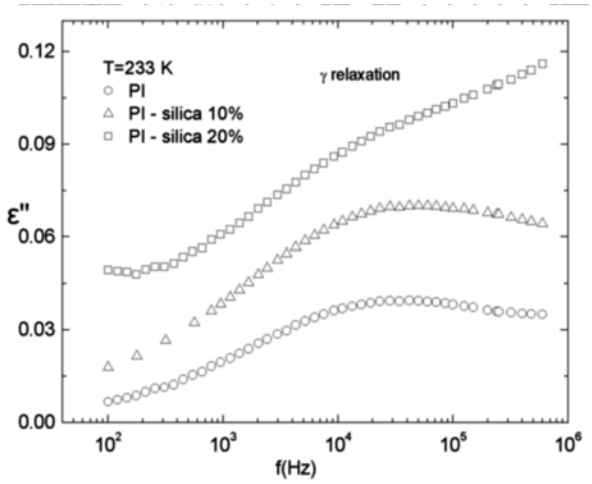

Fig. 4. Frequency dependence of dielectric losses ε'' of the PI/silica nanocomposites indicated on the plot in the region of the γ relaxation

and a temperature of -50°C) on volume concentration p of NCP in the inset to Fig. 2(a). The well-known equation for the dependence of ε' on p from percolation theory [12]

$$\varepsilon'(p) = \varepsilon'_m + A|p-p_c|^{-t} \quad (1)$$

where m refers to the matrix, p_c is the percolation threshold and t the critical exponent, has been fitted to the data and the values of p_c and t determined to 7.4% and 0.69 respectively. Two relaxations, a secondary β relaxation at lower temperatures and the primary α relaxation at higher temperatures, associated with the glass transition of the ER matrix, are observed in Fig. 2. They will be studied in more detail in following sections.

Fig. 3 shows results obtained with PI/silica nanocomposites prepared by the in situ generation of crosslinked organosilicon nanophase through the sol-gel process [11]. The step at higher frequencies is due to the secondary γ relaxation of the PI matrix. The most interesting result in Fig. 3 is the overall and monotonous decrease of ε' with increasing filler content. Moreover, the values are lower than those of bulk silica (ε' = 3.8 – 4.0), suggesting a looser molecular packing of PI chain fragments adjacent to the filler particles and/or a loose inner structure of the spatial aggregates of the organosilicon nanophase. By assuming a constant value of ε' for the PI matrix (ε'_m = 3.18) and by using various effective medium theory formulae for the calculation of the dielectric function of a composite material [11, 12] we obtained for the organosilicon nanophase ε'_i values between 2.47 and 1.58, depending on the composition and the specific formula used. The ε'_i values show, however, the same trend with composition, independently of the formula used. These results can be rationalized assuming that the organosilicon nanophase is made up of nanoparticles of silica (ε'_m = 3.8 – 4.0) fused together into loose spatial aggregates with a considerable fraction of empty inner pockets (ε'_i = 1). Effective medium theory calculations for this silica-air composite give for the volume fraction of air values in the range 0.40 – 0.65 [11].

3.2. Secondary relaxations

The step in ε'(f) in Fig. 3 at frequencies higher than about 10^4 Hz is due to the local γ relaxation of the PI matrix, tentatively attributed to non-cooperative motion of the imide groups and/or adsorbed water [10]. Fig. 4 shows results for the same γ relaxation in another series of PI/silica nanocomposites, prepared also by sol-gel techniques [10]. The magnitude of the relaxation increases with increasing silica content, without any change of the time scale (frequency position of the relaxation). Similar results were obtained by TSDC measurements.

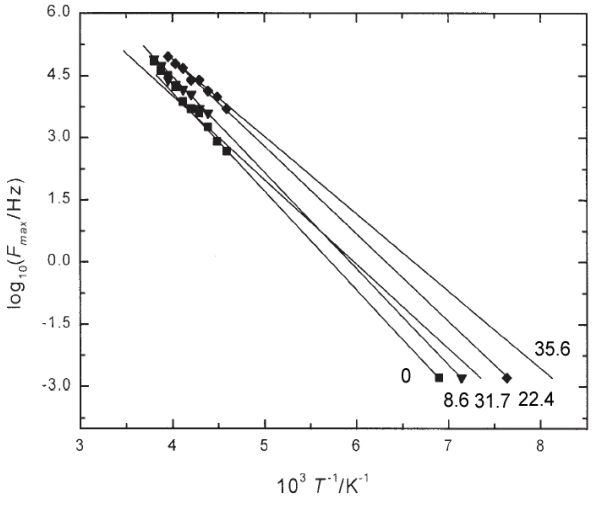

Fig. 5. Arrhenius plot for the γ relaxation in PI/silica nanocomposites. The numbers refer to the weight fraction of silica.

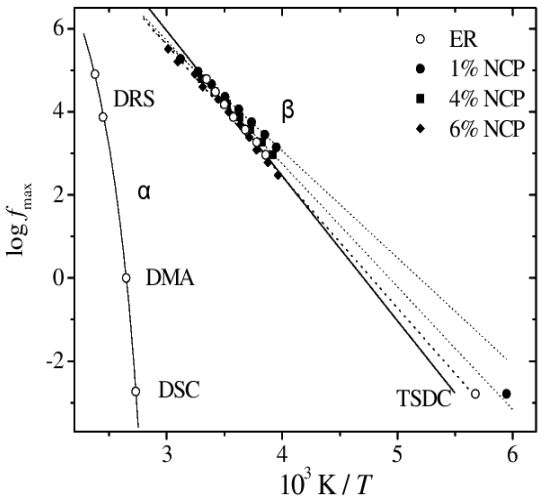

Fig. 6. Arrhenius plot for the α and β relaxation in the materials indicated on the plot. The lines are fits of the VTF and the Arrhenius equations, respectively, to the experimental data.

Measurements on the same PI/silica samples at different water contents by DS and by TSDC show that the frequency/temperature position of the γ peak does not change with water content, whereas its magnitude increases. These results indicate that adsorption of water has the same effect on the γ relaxation as the increase silica content. The effects of water in Pis are commonly explained in terms of plasticization and increase of free volume [10]. Thus, our results suggest that the same explanation may apply for the effects of silica inclusions on the local-scale dynamics in PIs. In addition, the magnitude of the γ relaxation does not extrapolate to zero for zero water content, suggesting a contribution of imide groups to the relaxation [10].

Analysis of the various relaxation mechanisms in the nanocomposites under investigation was done by fitting an appropriate function to the experimental data, typically the Havriliak-Negami function [6,7]

$$\varepsilon(f) - \varepsilon_\infty = \frac{\Delta\varepsilon}{[1+(i2\pi f/f_{HN})^{1-a}]^b} \tag{2}$$

.where Δε is the relaxation strength, ε∞ is the limit of ε'(f) to high frequencies, f_{HN} is a characteristic frequency close to the f_{max} of maximum dielectric loss, and a and b are shape parameters (b=1 for secondary relaxations which are expected to be symmetric [6,7]). The fitting parameters f_{HN}, (and f_{max}), Δε and a and b provide information on the time scale, the magnitude and the shape of the response.

As an example of the analysis, Fig. 5 shows the Arrhenius plot (activation diagram) of the γ relaxation for the PI/silica nanocomposites of Fig. 3. The plot includes DS data at high frequencies / temperatures and TSDC data at the equivalent frequency of 1.6 mHz corresponding to a relaxation time of 100 s [11]. The results show that the relaxation becomes faster in the nanocomposites. The Arrhenius equation [6,7]

$$f_{max} = f_0 \exp(-E_{act}/kT) \tag{3}$$

where E_{act} is the apparent activation energy, f_0 the pre-exponential frequency factor and k Boltzmann's constant, was fitted to the data and E_{act} and f_0 determined for each composition. Both E_{act} and f_0 tended to decrease with increasing filler content, from E_{act} = 49 kJ/mol and $\log f_0$ = 14.1 in pure PI to E_{act} = 36 kJ/mol and $\log f_0$ = 12.2 in the composite with 35.6wt%

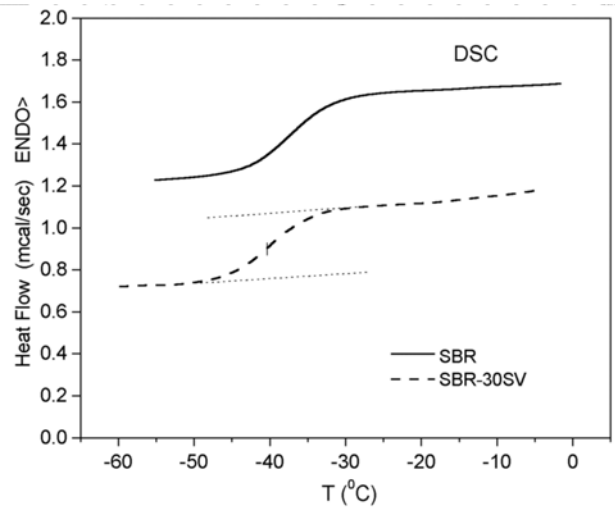

Fig. 7. Comparative DSC thermograms recorded for two SBR/silica samples indicated on the plot in the region of the glass transition at a heating rate of 20°C/min

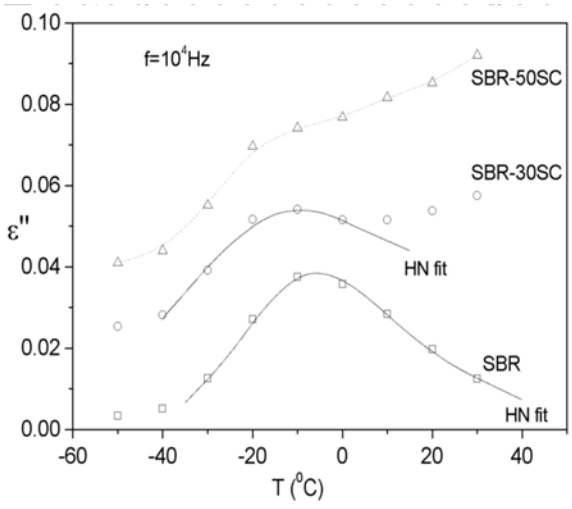

Fig. 8. Isochronal (constant frequency, f=10^4Hz) plot of dielectric loss ε" against temperature T in the region of the α relaxation for three SBR/silica samples indicated on the plot

organosilicon nanophase. These results are in agreement with the hypothesis of increased free volume in the nanocomposites due to loosened molecular packing of the chains close to the nanoparticles. Calculations have indicated a decrease of polymer density around a sphere, in particular for short chains [13]. Measurements have shown that the self-diffusion constant of pentane in a high-permeability polymer increases on addition of nanoparticles, and this result has been explained in terms of increased free volume [14].

Fig. 6 shows the Arrhenius plot for the ER/NCP composites of Fig. 2. The β relaxation in ER has been associated with motions of the hydroxypropylether group [15]. The magnitude of the relaxation increases in the nanocomposites, whereas the time scale (temperature position) of the response does not change appreciably with the composition, similarly to the results for the PI/silica nanocomposites of Fig. 4. The Arrhenius plot provides more details on the dynamics of the β relaxation. Similarly to the results in Fig. 5, the apparent activation energy in the Arrhenius equation (3) decreases in the nanocomposites (69 kJ/mol in ER, 51, 59, 63 kJ/mol in the nanocomposites with 1, 4, 6% NCP respectively), as does the corresponding frequency factor.

3.3. Primary α relaxation and glass transition

Figs. 7 and 8 refer to the SBR/silica nanocomposites of Fig. 1 and show results related to the glass transition. Fig. 7 show representative DSC thermograms obtained with SBR and SBR-30SV. The glass transition temperature T_g (onset and midpoint) and the heat capacity jump ΔC_p at the glass transition were determined from such thermograms following common procedures. T_g was found to decrease slightly and ΔC_p to decrease more than additivity would predict in the nanocomposites with respect to the pure matrix. The shift of T_g is systematically larger for the pretreated than for the non-treated samples. The shape of the response (the temperature range of the glass transition) did not practically change with respect to pure SBR. No second glass transition is observed at higher temperatures, as suggested by DMTA on the same samples [4]. These results can be understood in terms of two opposite effects [10]: immobilization of a fraction of chains at the interfaces, because of chemical bonds to the particles, which causes a deficit in ΔC_p, and loosened molecular packing of the chains, because of tethering and of geometrical confinement, which leads to increase of free volume and increased chain mobility. Interestingly, the shift of T_g is larger for the pretreated samples, in agreement with a lower degree of aggregation of nanoparticles in these samples, as indicated by the results in Fig. 1.

Fig. 8 shows isochronal ε"(T) plots for the samples of Figs. 1 and 7 in the region of the

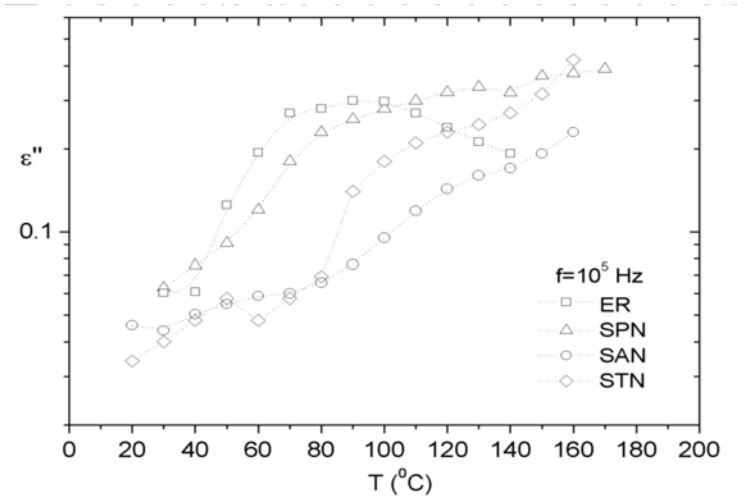

Fig. 9. Dielectric loss ε" against temperature T of the ER/clay samples indicated on the plot at 10^5 Hz.

primary α relaxation associated with the glass transition. For SBR and SBR-30SC a HN expression was fitted to the data. Following an evaluation method proposed by Schoenhals and coworkers [16], this was done by using the HN function in the frequency domain (Eq. (2)) and treating all parameters as temperature dependent. The results in Fig. 8 suggest, in agreement with those of DSC on the same samples, that the relaxation shifts slightly to lower temperatures in the nanocomposites without any broadening of the response, whereas they are less conclusive with respect to the magnitude of the relaxation.

Different results than those in Figs. 7 and 8 were obtained for ER/clay nanocompositesprepared by dispersing an organically modified smectite clay in a low viscosity ER (Araldite) [8]. Three types of alkaline cations were used for modification of samples prepared with about 5wt% smectite clay: SAN – $[(C_{16}H_{33})_x(C_{18}H_{37})_yN^+(CH_3)_2]$ (x = 0.5, y = 1.5); STN – $[(C_8H_{17})_3(CH_3)N^+]$ and SPN – $[(C_2H_5)_2(CH_3)N^+(O\text{-}iPr)_{25}]$. The results in Fig. 9 for the primary α relaxation suggest a shift of the relaxation, i.e. of the glass transition temperature, to higher temperatures in the nanocomposites. Similar results were obtained also with the ER/NCP nanocomposites of Fig. 2: the α relaxation peak temperature increases slightly in the nanocomposites, in particular at higher filler contents, where it shifts out of the temperature range of measuremets. These results suggest that in these systems immobilization of a fraction of chains at the interfaces dominates over increased free volume effects.

The limited amount of data for the α relaxation in the ER/NCP nanocomposites, due to strong conductivity effects at higher temperatures, did not allow to study in detail the dynamics of the relaxation. For that reason, the Arrhenius plot for this relaxation is shown only for the pure ER matrix in Fig. 6. DMA (at 1 Hz) and DSC data (at the equivalent frequency of 1.6 mHz of TSDC data [17]) allow to expand the frequency/temperature range of the presentation. The Vogel-Tammann-Fulcher (VTF) equation [6,7,17]

$$f_{max} = A \exp[-B/(T-T_0)] \qquad (4)$$

with temperature independent empirical parameters A, B and T_0, was fitted to the data with reasonable values of the fitting parameters.

Thus, our results show that in the various nanocomposites studied T_g may decrease or increase, with respect to the pure polymer matrix. Similar results have been reported in the literature, e.g.: two T_gs, one for the unmodified polymer matrix and a higher one for the polymer close to the filler particles [2,4]; reduction of T_g [18, 19]; no change of T_g [20]; increase of T_g [21]; dependence of T_g on the morphology for clay nanocomposites [22,23].

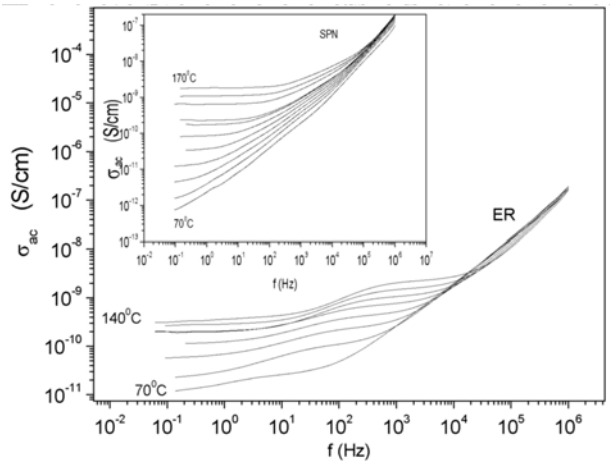

Fig. 10. Real part of ac conductivity σ_{ac} against frequency f for the ER matrix at temperatures between 70 and 140°C in steps of 10°C. The inset shows a similar plot for the SPN nanocomposite in the range 70 – 170°C.

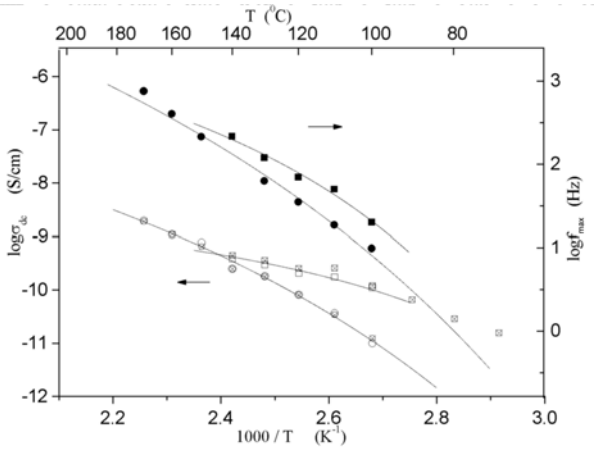

Fig. 11. Arrhenius plot of the frequency f_{max} of the CCR process (filled symbols) and of dc conductivity σ_{dc} obtained by a fitting procedure [8] (open symbols) and from the σ_{ac} plots in Fig. 10 (open crossed symbols) for the ER matrix (squares) and the SPN nanocomposite (cicrles).

3.4. Conductivity effects

Figs. 10 and 11 show results on dc conductivity and conductivity effects obtained with ER/clay nanocomposites treated with SPN. The ac conductivity σ_{ac} plotted against frequency in Fig. 10 and in the inset to Fig. 10 for the pure ER matrix and the SPN nanocomposite, respectively, has been obtained from ε"(f) by

$$\sigma_{ac}(f) = 2\pi f \varepsilon_0 \varepsilon''(f) \quad (5)$$

where ε_0 is the permittivity of free space. The plot for ER exhibits a dc conductivity plateau at low frequencies / high temperatures and a step at 10^1 – 10^3 Hz, corresponding to a conductivity current relaxation (CCR). The latter is assigned to the accumulation and relaxation of charges at the interfaces between regions of different conductivity under conditions of dc conductivity for the sample as a whole [8]. The presence of CCR suggests a large scale heterogeneity of the structure of the ER matrix, in agreement with results obtained by other techniques [15, 24]. Several changes are observed in the plot for the nanocomposite with respect to that of the pure matrix: the dc conductivity plateau is observed at higher temperatures, suggesting a shift of T_g to higher temperatures, in agreement with the results for the α relaxation in Fig. 9; the dc conductivity values are, for the same temperature and T ≤ 150°C, lower, in agreement with increased barrier properties of these nanocomposites [1,25]; the CCR relaxation becomes weaker, suggesting that the corresponding heterogeneity becomes less pronounced on addition of the nanoparticles.

The Arrhenius plot in Fig. 11 includes data for the dc conductivity σ_{dc} obtained by a fitting procedure to ε"(f) data not shown here [8] and from the σ_{ac}(f) plots of Fig. 10, in good agreement with each other, and for the peak frequency f_{max} of the CCR relaxation. The VTF equation (4) was fitted to the CCR data and a similar equation to the σ_{dc} data. The satisfactory fits suggest that both processes are connected to the α relaxation (dynamic glass transition), with the charge carrier transport being governed by the motion of the polymeric chains. Moreover, the results in Figs. 9 – 11 indicate that the overall mobility is decreased in the nanocomposites as compared to the pure ER matrix, in the temperature range studied, providing a basis for understanding the observed increased thermal stability in polymer-clay

nanocomposites [1,25]. It is interesting to note the different dynamics of charge carrier transport in the nanocomposites, as compared to the pure matrix. The higher values of dc conductivity in the nanocomposites at T≥ 150 ^{o}C suggested by Fig. 11 may results from a higher concentration of charge carriers due to mixing with the clay and the modifier.

4. CONCLUSIONS

Dielectric spectroscopy (DS) in the frequency domain and thermally stimulated depolarization currents (TSDC) techniques, covering together a broad frequency range (10^{-4} – 10^{9} Hz), were employed to investigate molecular dynamics and to deduce on morphology in polymeric nanocomposites. Several systems were investigated including epoxy resin-modified smectite clay nanocomposites of exfoliated structure (ER/clay), epoxy resin-carbon particle nanocomposites with a mean particle diameter of 3nm (ER/NCP), styrene-butadiene rubber-silica nanocomposites (SBR/silica) and polyimide-silica nanocomposites prepared by sol-gel techniques (PI/silica).

The results proved that dielectric techniques are very powerful for investigating molecular dynamics in relation to morphology in nanocomposites. The broad frequency region covered allows to obtain information from local secondary relaxations and from the cooperative, primary α relaxation associated with the glass transition of the polymer matrix, as well as from conductivity effects related to the microscopic and macroscopic charge carrier transport in the nanocomposite. Detailed analysis of each of the relaxation mechanisms studied provides information on the time scale, the magnitude (relaxation strength) and the shape of the response, which can be related to specific aspects of the structure and the morphology of the nanocomposite. In addition, information on the degree of agglomeration of the nanoparticles and the internal structure of the agglomerates can be obtained from an effective medium analysis of the dielectric data.

Several interesting results were obtained with each of the four systems studied and discussed in relation to results obtained by using other techniques. We would like to stress here three observations, which may apply for more systems. (i) Electrical conductivity effects recorded over a broad frequency / temperature range provide significant information on morphology, as the moving ions probe the local morphology, whereas dc conductivity values provide information on barrier properties. (ii) Chemical treatment of the nanoparticles and/or details of the method of preparing the nanocomposites are reflected in the characteristics of the cooperative segmental relaxation and in conductivity effects, such as space charge polarization and conductivity current relaxation. (iii) The frequency/temperature position of local, secondary relaxations of the polymer matrix is not significantly altered by the presence of the nanoparticles. However, in two of the systems studied (PI/silica and ER/NCP) the dynamics changed a lot, with both the apparent activation energy and the pre-exponential factor in the Arrhenius equation decreasing significantly in the nanocomposites. This point will be further followed in other nanocomposites.

Several of the results obtained within this and previous work on changes in the molecular dynamics of the polymeric matrix induced by the presence of the filler nanoparticles can be understood in terms of two opposite effects: immobilization of a fraction of chains at the interfaces, due to chemical or physical bonds to the particles, and loosened molecular packing of the chains due to tethering and geometrical confinement, resulting in an increase of free volume.

References

1. **Alexandre, M.** and **Dubois, P.**, "Polymer-layered silicate nanocomposites: preparation, properties and uses of a new class of materials", *Mater. Sci. Eng.*, **28** (2004), 1-63.
2. **Tsagaropoulos, G.** and **Eisenberg, A.**, "Dynamic mechanical study of the factors affecting the two glass transition behavior of filled polymers. Similarities and differences with random ionomers", *Macromolecules*, **28** (1993), 6067-77
3. **Berriot, J.**, **Montes, H.**, **Lequeux, F.**, **Long, D.** and **Sotta, P.**, "Evidence for the shift of the glass transition temperature near the particles in silica-filled elastomers", *Macromolecules*, **35** (2002) 9756-62

4. **Arrighi, V.**, **McEwen, I.J.**, **Qian, H.** and **Serrano Prieto, M.B.**, "The glass transition and interfacial layer in styrene-butadiene rubber containing silica nanofiller", *Polymer*, **44** (2003) 6259-66
5. **Litvinov, V.M.**, **Barthel, H.** and **Weis, J.**, "Structure of a PDMS layer grafted onto a silica surface studied by means of DSC and solid-state NMR", *Macromolecules*, **35** (2002), 4356-64
6. **Hedvig, P.**, "Dielectric spectroscopy of polymers", Adam Hilger, Bristol (1977)
7. **Runt, J.P.** and **Fitzgerald, J.J.**, Eds., "Dielectric spectroscopy of polymeric materials", American Chemical Society, Washington, DC (1997)
8. **Kanapitsas, A.**, **Pissis, P.** and **Kotsilkova, R.**, "Dielectric studies of molecular mobility and phase morphology in polymer-layered silicate nanocomposites", *J. Non-Cryst. Solids* **305** (2002), 204-11
9. **Kotsilkova, R**., **Fragiadakis, D.** and **Pissis, P.**, "Reinforcement effect of carbon nanofiller in epoxy resin systems: rheology, molecular dynamics and mechanical studies", submitted to *J. Polym. Sci. Part B: Polym. Phys.*
10. **Bershtein, V.A.**, **Egorova, L.M.**, **Yakushev, P.N.**, **Pissis, P.**, **Sysel, P.** and **Brozova, L.**, "Molecular dynamics in nanostructured polyimide-silica hybrid materials and their thermal stability", *J. Polym. Sci. Part B: Polym. Phys.* **40** (2002), 1056-69
11. **Kramarenko, V.Y.**, **Shantalii, T.A.**, **Karpova, I.L.**, **Dragan, K.S.**, **Privalko, E.G.**, **Privalko, V.P.**, **Fragiadakis, D.** and **Pissis, P.**, "Polyimides reinforced with the sol-gel derived organosilicon nanophase as low dielectric permittivity materials", *Polym. Adv. Technol.* **15** (2004), 144-8
12. **Pelster, R.** and **Simon, U.**, "Nanodispersions of conductive particles: preparation, microstructure and dielectric properties", *Colloid Polym. Sci.* **277** (1999), 2-14
13. **Tuinier, R.** and **Lekkerkerker, H.N.W.**, "Polymer density around a sphere", *Macromolecules*, **35** (2002), 3312-3
14. **Zhong, J.**, **Wen, W.-Y.** and **Jones, A.A.**, "Enhancement of diffusion in a high-permeability polymer by the addition of nanoparticles", *Macromolecules*, **36** (2003), 6430-32
15. **Maggana, C.** and **Pissis, P.**, "TSDC studies of the effects of plasticizer and water on the sub-T_g relaxations of an epoxy resin system", *J. Macromol. Sci.-Phys. B*, **36** (1997), 749-772
16. **Schlosser, E.**, **Schoenhals, A.**, **Carius, H.-E.** and **Goering, H.** "Evaluation method of temperature-dependent relaxation behavior of polymers", *Macromolecules*, **26** (1993), 6027-32
17. **Donth, E.**, "Relaxation and thermodynamics. Glass transition", Akademie, Berlin, 1992
18. **Van Asche, G.** and **Van Mele, B.**, "Interphase formation in model composites studied by micro-thermal analysis", *Polymer*, **43** (2002), 4605-10
19. **Zhou, S.**, **Wu, L.**, **Sun, J.** and **Shen, W.**, "The change of the properties of acrylic-based polyurethane via addition of nano-silica", *Progr. Org. Coat.*, **45** (2002), 33-42
20. **Torro-Palau, A.M.**, **Fernandez-Garcia, J.C.**, **Orgiles-Barcelo, C.** and **Martin-Martinez, J.M.**, "Characterization of polyurethanes containing different silicas", *Int. J. Adhes. Adhes.*, **21** (2001), 1-9
21. **Lu, H.** and **Nutt, S.**, "Enthalpy relaxation of layered silicate-epoxy nanocomposites", *Macromol. Chem. Phys.*, **204** (2003), 1832-41
22. **Kinloch, A.J.** and **Taylor, A.C.**, "Mechanical and fracture properties of epoxy-inorganic micro- and nanocomposites", *J. Mater. Sci. Lett.*, **22** (2003), 1439-41
23. **Ellis, T.S.** and **D'Angelo, J.S.**, "Thermal and mechanical properties of a polypropylene nanocomposite", *J. Appl. Polym. Sci.*, **90** (2003), 1639-47
24. **Kontou, E.**, **Spathis, G.** and **Theocharis, P.S.**, "The heterogeneity of the network structure of epoxy polymers studied by dynamic and DSC tests", *J. Polym. Sci. Polym. Chem. Ed.*, **23** (1985), 1493-1503
25. **Giannelis, E.P.**, "Polymer layered silicate nanocomposites", *Adv. Mater.*, **8** (1996) 29-35